Available online at www.sciencedirect.com
ScienceDirect
Journal of Sound and Vibration 321 (2009) 875–892
JOURNAL OF SOUND AND VIBRATION
www.elsevier.com/locate/jsvi

Spectra and directivity of a Hartmann whistle

S. Narayanan, P. Bhave, K. Srinivasan*, K. Ramamurthi, T. Sundararajan

Department of Mechanical Engineering, Indian Institute of Technology Madras, Chennai 600036, India

Received 22 December 2006; received in revised form 24 October 2008; accepted 29 October 2008
Handling Editor: J. Lam
Available online 16 December 2008

Abstract

Experimental and theoretical studies of the spectral and directivity characteristics of a Hartmann whistle are presented for pressure ratios in the range of 4.92–6.88. Cavity resonance is observed for the range of pressure ratios studied and the sound pressure amplitudes are larger than those of free jets. Distinct spectra with high sound pressure levels are observed at the fundamental frequency as well as the higher harmonics. Based on dimensional analysis, an expression for the fundamental frequency is derived in terms of the stagnation sound speed, cavity length, and stand-off distance. The analogy between Hartmann whistle and a classical Helmholtz resonator is discussed. Numerical simulations of the flow field, carried out to supplement the experimental findings, show that the jet regurgitance is significant at smaller values of cavity-stand-off distances. The correspondence between flow pattern seen from numerical simulations and the maximum directivity observed from acoustical measurements is highlighted. The flow diversion around the cavity explains the observed shift in directivity towards higher angles for the whistle, as compared to the free jet flow. The acoustic power and efficiency are high for small values of stand-off distances and larger cavity lengths.

1. Introduction

Cavities placed in high speed flows can serve as high intensity, narrow band acoustic sources with selective directivity. Such sources can be gainfully used to control the flow, mixing and combustion processes in various propulsion applications. The present study experimentally investigates the directivity and spectral characteristics of the Hartmann–Sprenger tube or 'Hartmann whistle' comprising a cylindrical tube placed against a high speed jet flow. The modification introduced by the cavity in the jet flow acoustics are determined and interpreted with the help of a simplified cavity resonator model and supplemented by numerical simulations.

The high intensity noise generated in a Hartmann whistle has been classified into three distinct regimes [1] comprising the jet instability mode (JIM), the jet regurgitant mode (JRG), and the screech mode (SCM). The screech is a high frequency mode, which occurs due to the feedback loop generated due to the interaction of shock cells with vortices convected in the mixing layer. This mode has been shown to occur for large values of nozzle pressure ratio $R \geqslant 3.9$ [1]. The JRG occurs due to the periodic swallowing and discharging of jet flow by

*Corresponding author. Tel.: +91 44 2257 4703; fax: +91 44 2257 4652.
E-mail address: ksri@iitm.ac.in (K. Srinivasan).

0022-460X/$ - see front matter © 2008 Elsevier Ltd. All rights reserved.
doi:10.1016/j.jsv.2008.10.023

Nomenclature

A_{neck}	cross section area of the neck, m^2
a_1, a_2	constants obtained from experiments
C	speed of sound in ambient air, m/s
D_c	cavity diameter, m
D_j	jet diameter, m
f	frequency, Hz
f_{sfj}	frequency of screech in free jet, Hz
H	Helmholtz number ($=fL/C$)
L	cavity length, m
L_{neck}	length of the neck, m
M_j	Mach number at the exit of the nozzle
$\dot{m}$	mass flow rate through the nozzle, kg/s
n	Harmonic index; 1 (fundamental) (2,3,… higher harmonics)
p_0	stagnation pressure, N/m^2
p_a	ambient pressure, N/m^2
P	acoustic power, W
r	radius of sphere for defining slice power (Eq. (1)), m
r_c	correlation coefficient between two variables
R	nozzle pressure ratio ($=p_0/p_a$)
S	stand-off distance, m
St	Strouhal number ($=fD_j/U_j$)
U_j	jet velocity at nozzle exit, m/s
y^+	dimensionless distance from the wall
V	volume of the air in the Helmholtz resonator, m^3
θ	polar angle, degrees
Π	non-dimensional parameter
ρ	density, kg/m^3
SPL	sound pressure level, dB re 20×10^{-6} Pa

the cavity at the fundamental cavity resonance frequency. The JIM is driven at lower jet speeds corresponding to $R<1.9$. In this mode, large toroidal vortices that are shed periodically at the nozzle exit grow in size as they are convected downstream, and cause weak compression waves inside the cavity. The frequency of oscillations in this mode has been shown to be governed by the jet Strouhal number (fD_j/U_j) around 0.3 [1]. The investigations by Brocher et al. [2] on the JRG mode revealed that the maximum amplitude of oscillations is obtained when the stand-off distance (S) is equal to the diameter of the resonant cavity (D_c) for subsonic flows, and twice the diameter for supersonic flows. SCM is obtained when S is considerably greater than D_c. Iwamoto [3] concluded that the necessary conditions for initiating and maintaining a stable resonance in a Hartmann cavity are the existence of a positive pressure gradient near the open end of the cavity and a low-pressure region on the outside surface of the cavity wall.

Sobeiraj and Szumowski [4] observed that while the shape of the cavity edge considerably affects the acoustical/thermal phenomena and oscillatory modes (screech and regurgitant switching), the shape of the nozzle exit edge is almost insignificant. The frequency corresponding to the SCM is also seen to be higher than that of the regurgitant mode in the range $2<R<3.5$. For $R>4$, the SCM dominates for small stand-off distances and the regurgitant mode for large stand-off distances. Kastner and Samimy [5] developed a Hartmann cavity in which a major portion of the region between the jet and the cavity is shielded so that the pulsating jet could be used for flow control. They observed that the stand-off distance between the jet and the cavity is a crucial parameter for effective flow control.

Two distinct characteristic tones were observed by Raman et al. [6]. One scales with flow and is characterized by $H=0.3nM_j^{1/2}$, where H is the Helmholtz number given by fL/C, n is the harmonic index and M_j is the Mach number at the exit of the nozzle. The other tone originates from cavity acoustics and is depicted by $H\approx(2n-1)/4$.

The parametric study of Sarpotdar et al. [7] revealed that at $R=4.29$, the characteristic frequency remains almost constant regardless of the stand-off distance. It was also observed that the fundamental frequency radiates mainly in the downstream direction of the jet for low values of the characteristic frequencies.

Raman et al. [8] provided the detailed characterization of the unsteady pressures in the near-field. The frequencies predicted by the quarter wavelength formula were in good agreement with the measured values for longer cavity lengths but the formula was found to be increasingly inaccurate for smaller cavity lengths. Gregory and Sullivan [9] used pressure-sensitive paint (PSP) to explore the relationship between the unsteady flow field and acoustics of the cavity. The nature of the shock oscillations, unsteady flow interactions and directionality of the radiated sound were analyzed. Their results agreed with those of Brun and Boucher [10].

Murugappan and Gutmark [11] observed that there was a mode switch from screech to JRG at very low stand-off distances ($S/D_j<0.8$). The JRG was observed to sustain over a wide range of S for a cavity to jet diameter, $D_c/D_j>1$. Diameter ratios $D_c/D_j<1$ sustained high frequency SCMs for a wide range of cavity parameters. Brun and Boucher [10] also found that when the ratio D_c/D_j is larger by a factor of 1.33–2.5, the intensity of sound emitted is high. Hamed et al. [12,13] investigated numerically, the effect of cavity geometry on the unsteady flow characteristics and mass flow variations in a resonance cavity. The whistle exhibits JRG modes at lower Mach numbers and SCMs at higher Mach numbers. In the JRG mode, the fundamental frequency agrees with the cavity quarter wave frequency. Chang et al. [14] studied the Hartmann cavity flow driven by an underexpanded sonic jet by solving the axisymmetric Euler equations using the total variation diminishing (TVD) scheme. The generation of shock and expansion waves in the whistle and their interactions with the impinging jet were described through the four sequential phases of intake, transition to expulsion, expulsion, and transition to intake.

It is evident from the literature that there is a sustained interest in understanding the mechanisms in a Hartmann whistle. In applications such as flow and noise control, it is important to fully understand the spectral and directivity characteristics of the whistle (flow impinging on a cavity) for proper deployment. Experimental and numerical studies are carried out in the present investigation to understand and model the spectral and directivity characteristics. The specific objectives of the work are: (i) to investigate the modifications in jet flow acoustics in the presence of the cavity, (ii) to develop a frequency prediction model, and (iii) to obtain the tonal and overall directivities as well as power directivity.

2. Experimental set up and procedure

2.1. Hartmann whistle and jet flow facility

A convergent nozzle of 7 mm exit diameter attached at the end of a settling chamber, produces an underexpanded jet corresponding to $4.92<R<6.88$. The jet impinges at the open end of a cylindrical cavity which is closed at the rear end. The cavity length is varied by an adjustable leak-proof piston capable of sliding inside the cavity. The inner diameter of the cavity is 7 mm and the outer diameter is 17 mm. The dimensions of the nozzle and cavity are shown in Fig. 1.

The cavity is mounted on a linear traverse for varying the stand-off distance with respect to the jet flow. In order to ensure good alignment between the axes of the nozzle and cavity, the piston whose diameter is slightly less than that of the nozzle exit, was inserted coaxially into the nozzle by adjusting the traverse. The height could be varied using the traverse. The nozzle and cavity are housed in an anechoic chamber as illustrated in Fig. 2.

A 150-hp two-stage reciprocating compressor is used to generate pressures up to 0.8 MPa and the high pressure air is stored in two tanks of total capacity 20 m^3. A settling chamber is connected to the high pressure air through 4 in plumbing and a needle valve is used to control the flow rate into the settling chamber. A pressure gauge (Bourdon type, range: 0–1.4 MPa) is mounted on the settling chamber to monitor the pressure. In order to eliminate structure-borne acoustic disturbances, a polyurethane foam lining is provided along the inner walls of the settling chamber. Two wire mesh screens of progressive fineness are placed in the settling chamber.

Since acoustical measurements require a free-field, an anechoic chamber has been built around the Hartmann-whistle. Polyurethane foam wedges are used as anechoic material on all the walls except the floor, to yield an overall working space of 2.5 m × 2 m × 2 m (tip-to-tip). The floor of the chamber is lined with a carpet, to minimize reflections from the ground. Two small windows, one each in the upstream and downstream directions enable the jet flow to freely entrain ambient air and exit the chamber without recirculation. The anechoic chamber is calibrated by verifying the inverse square law along various radial paths in the chamber, and is found to be anechoic above 630 Hz within ± 0.5 dB. The frequencies of interest lie above the lower cut-off frequency of the chamber, and therefore, the chamber is anechoic for the present set of experiments.

The range of parameters studied are as follows: length of the cavity is varied from $L/D_j = 4.28$ to 7.14 in steps of 0.71, stand-off distance S/D_j from 2.86 to 6.0, and nozzle pressure ratios R considered are 4.92, 5.91,

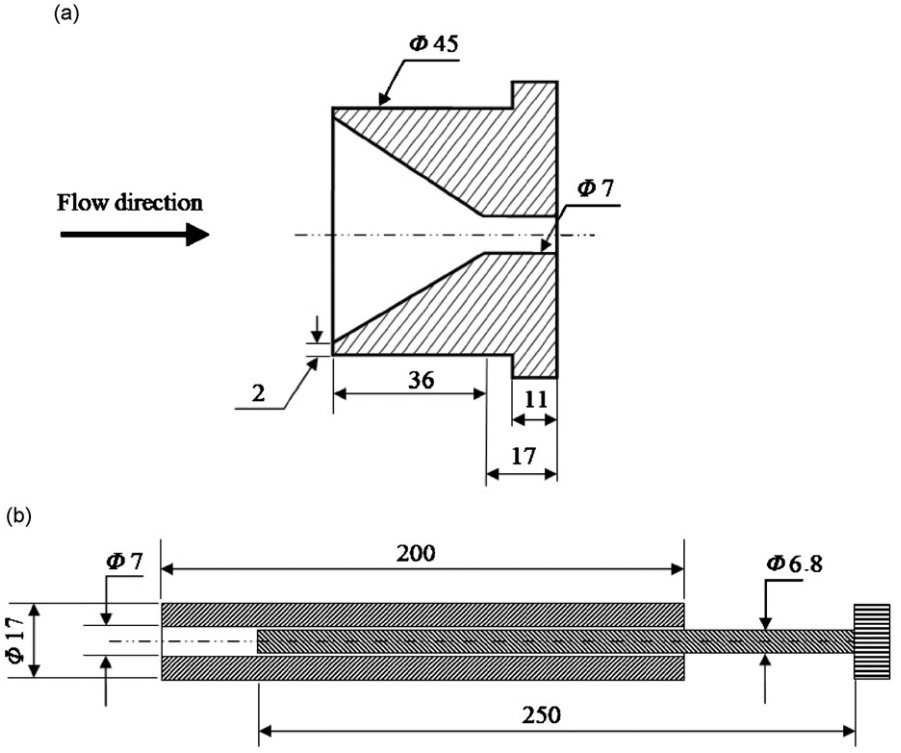

Fig. 1. Dimensions of nozzle and cavity: (a) nozzle and (b) cavity. (all dimensions are in mm).

and 6.88. The experimental and theoretical methodologies and the results obtained are presented in the subsequent sections.

2.2. Measurements, instrumentation and data processing

The acoustic measurements are made by a $\frac{1}{4}$in (6.35 mm diameter) condenser microphone (PCB Piezotronics, model no. 377A01), with an open circuit sensitivity of 4 mV/Pa at 250 Hz. The microphone has a flat response within 1 dB for the frequency bandwidth of 10 Hz–40 kHz. The microphone is attached to an angular traversing system capable of moving in a circular path with a pre-set range and step size. The stepper motor of the traverse is controlled by a stepper drive (National Instruments NI-MID-7604) and the motion is automated using LABVIEW 7.1 software. The movement of the traverse is such that the microphone always points towards the nozzle exit. The microphone signal is low-pass filtered at 70 KHz for anti-aliasing using an analog filter (Krohn-Hite, Model-3364). The microphone data is acquired for one second at a sampling frequency of 150 KHz, and transferred to a PC using an eight-channel (simultaneous sampling) data acquisition board (NI-PCI-6143). Data acquisition and motion control are synchronized using the same LABVIEW program. A record of 150 000 time-series data points was divided into FFT blocks of 4096 data points each (with zero padding, where necessary). The spectra obtained from each FFT block were averaged. The Hanning window is used for determining FFT.

The angular traverse moves the microphone in steps of 2° at a fixed radius of around $64D_j$ in the vertical plane. A restricted range of angles between 35° and 135° was adopted for the whistle to avoid interaction with the flow in the downstream portion and settling chamber upstream. The traverse starts its motion at an angle of 35° as measured from the downstream jet axis, in the anticlockwise direction. The microphone data obtained at each location (totally about 50 locations), is stored on the computer from which the spectra, intensity, tonal SPL (sound pressure level) and other variables are calculated using scripts written in

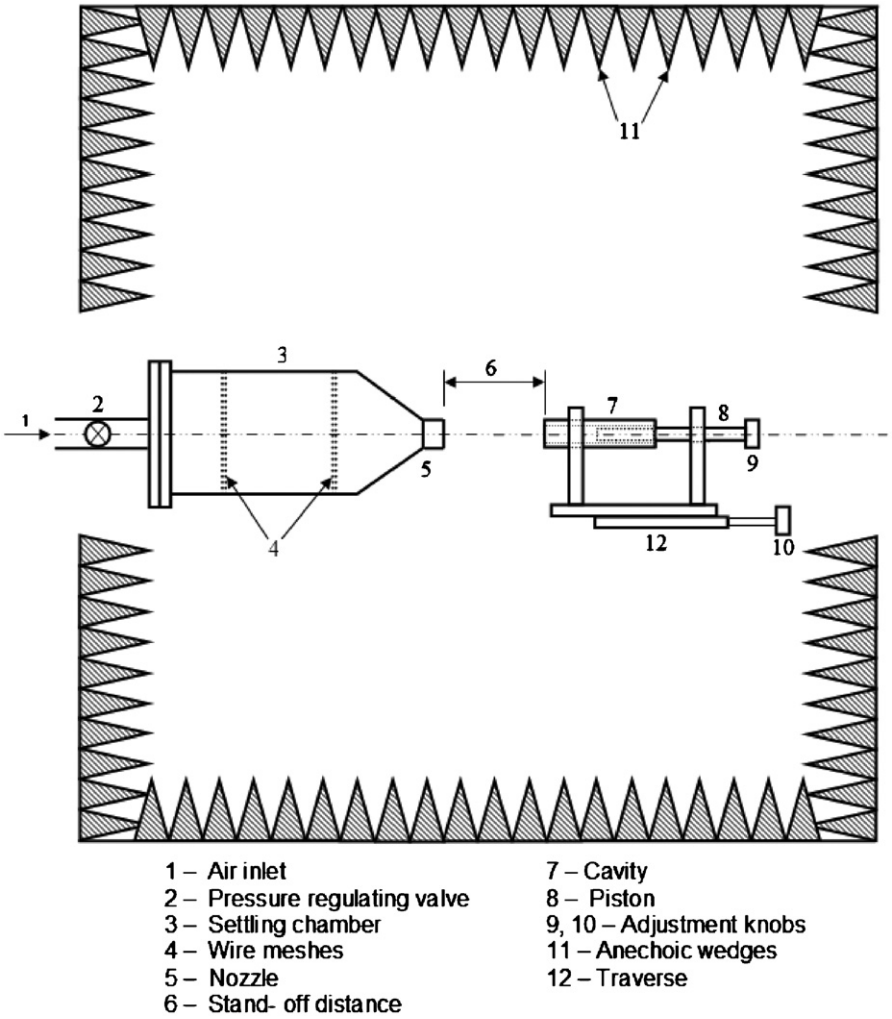

Fig. 2. Experimental setup.

MATLAB 7.0 software. Since the experiments are conducted in a free field environment, the SPL and the sound intensity level (SIL) are identical. The acoustic power in a given slice area termed as "slice power", is the product of the intensity and the corresponding slice area, as follows:

$$\text{Slice power} = \text{Intensity} \times 2\pi r^2 \int_{\theta_1}^{\theta_2} \sin\theta \, \mathrm{d}\theta \tag{1}$$

The total acoustic power is obtained by summing up the slice power over the entire spherical measurement surface.

The input power can be obtained as $\dot{m}U_j^2/2$, where $\dot{m}$ is the choked mass flow rate through the nozzle. The acoustic efficiency is the ratio of the output acoustic power to the input power. Tonal sound pressure levels corresponding to the fundamental frequency and higher harmonics are determined by integrating the respective areas under the power spectrum.

The uncertainty in the measurement of acoustic pressure was within ± 1 dB including repeatability factors. The frequency resolution in the spectra presented is within 37 Hz. The uncertainty in stagnation pressure

measurement was ±2%. The uncertainty in the measurement of stand-off distance and cavity length was within ±0.02 mm. The variation of ambient temperature inside the anechoic chamber was within ±1 K.

3. Frequency characteristics and theoretical modeling

3.1. Spectra comparison of Hartmann whistle and free jet

Firstly, the present results of a free jet are compared with those of Seiner [15] in Fig. 3. The SPLs, dominant Strouhal numbers are seen to match well. Minor deviations, seen in the figure, could be attributed to the fact that Seiner used convergent divergent nozzle whereas the present work employs a convergent nozzle in underexpanded mode. Further, the nozzle dimensions, measurement angles and locations, and anechoic environment are different in the two studies.

The acoustic spectra obtained at various values of θ (37°, 87°, and 135°), nozzle pressure ratio (R) of 4.92, stand-off distance (S/D_j) of 4.57 and cavity aspect ratio (L/D_j) of 4.28, are given in Fig. 4. The corresponding spectra of the free jet at $R = 4.92$ is also included in the figure for comparison. It is seen that the free jet screeches at this value of pressure ratio. The free jet screeching frequency is denoted as f_{sfj} and is indicated by the arrow in the figure. The presence of cavity in a screeching jet causes large sound pressure levels at frequencies lower than f_{sfj}. Since the feedback mechanism responsible for screech operates in the downstream-to-upstream direction, it is observed that the amplitude of the screech tone (f~15 kHz) at the far downstream/upstream angles (37°,135°) is greater than that at angles almost normal to the jet axis (87°). When the screech tone of the free jet is dominant (peaks being significantly higher than the base levels), the whistle exhibits higher degree of discreteness in the tones (fundamental and the harmonics). However, it may be observed that the values of fundamental frequency of the free jet and the whistle are not the same. The jet acoustics is essentially modified by the introduction of the cavity. Apart from the presence of new spectral components at low frequency levels, the sound pressure level over the entire audible frequency range is significantly enhanced due to the interaction with the cavity. The whistle, therefore, serves as an acoustic amplifier over the entire frequency range of interest (0–30 kHz).

The spectra at the same values of stand-off distance and cavity length but at a higher value of $R = 6.88$, are shown in Fig. 5. It is observed that the free jet does not screech at this pressure ratio, in agreement with Raman's screech cessation theory [16]. The values of the frequencies obtained by the interaction with the cavity, however, remains about the same.

The variations of the fundamental frequency with parameters L/D_j and different values of the stand-off distances S/D_j for R of 4.92 and 5.91 are shown in Fig. 6(a) and (b). The frequency falls rapidly as the length of the cavity increases. It is possible to tune the frequency by suitably adjusting the values of L/D_j and S/D_j. Experiments conducted for various nozzle pressure ratios gave similar trends. Frequency prediction, assuming resonance caused by the standing wave mode of a cavity open at one end and closed at the other ($f = C/4L$),

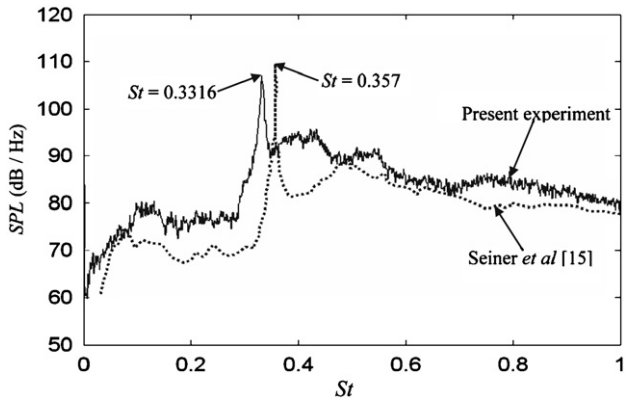

Fig. 3. Comparison of free jet spectrum obtained from present experiment at $R = 4.92$ with Seiner et al. [15].

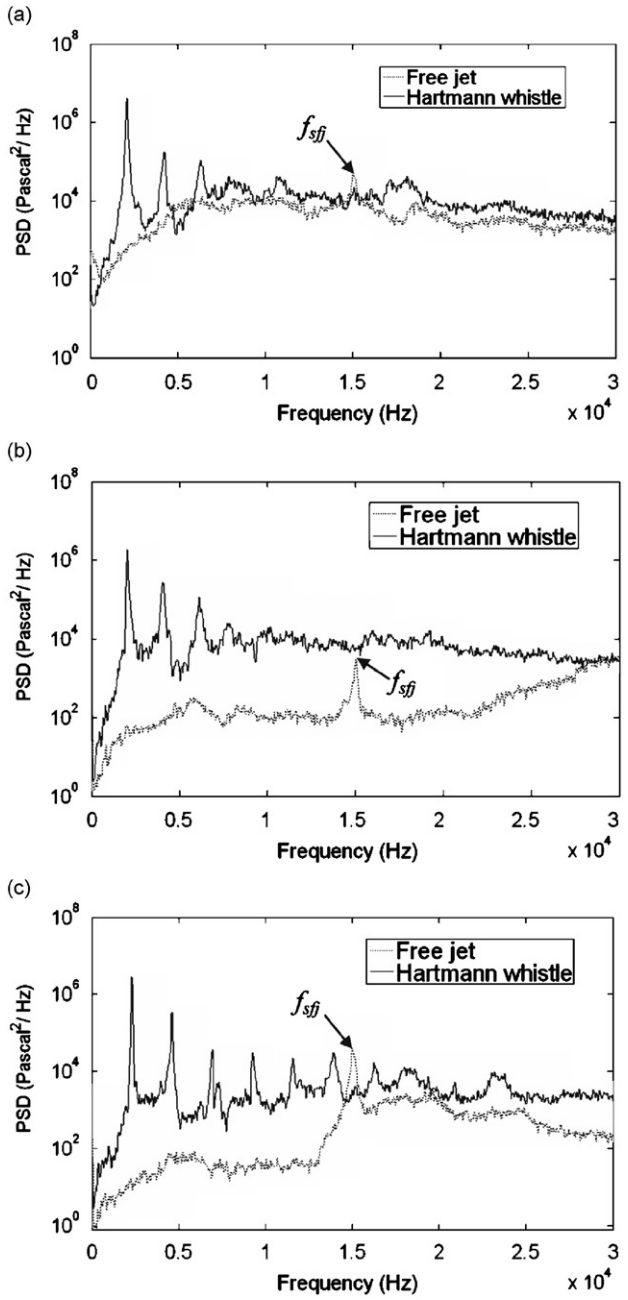

Fig. 4. Spectra comparison of Hartmann whistle ($S/D_j = 4.57$, $L/D_j = 4.28$) and free jet at $R = 4.92$ for three values of θ. (a) $\theta = 37°$; (b) $\theta = 87°$; and (c) $\theta = 135°$.

gives values which are significantly higher. This is shown as dark continuous line in Fig. 6(a) and (b). The earlier investigators (see for instance Refs. [2,17]) had attributed the deviations between experiments and predictions to the end-effects. A correction of the predicted frequency taking into account the end-effects [17] is shown as a dash-line in Fig. 6(a) and (b). The deviations, even after including the end-effects, are observed to be still large. The fundamental frequency variation with cavity length obtained from the present experiments at an S/D_j of 4.57 and $R = 4.92$ is compared with the results of Sarpotdar et al. [7] for $S/D_j = 1.5$ and $R = 4.29$ in Fig. 6(c). In spite of differences in the stand-off distance and the pressure ratio, the trends remain the same.

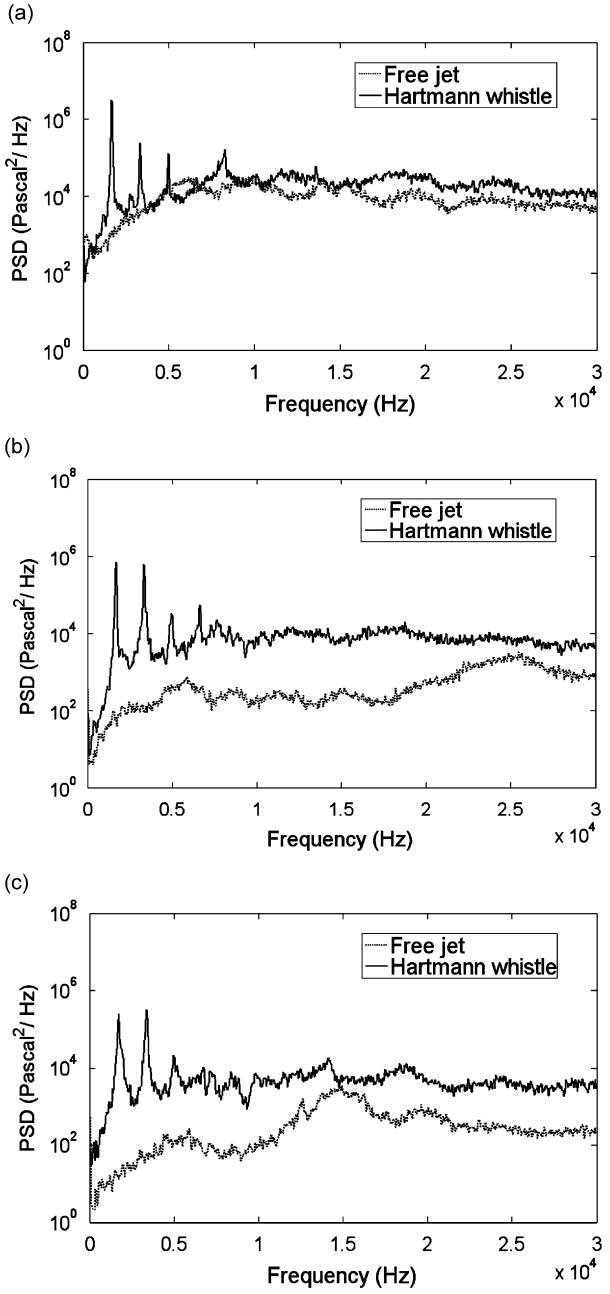

Fig. 5. Spectra comparison of Hartmann whistle ($S/D_j = 4.57$, $L/D_j = 4.28$) and free jet at $R = 6.88$ for three values of θ. (a) $\theta = 37°$; (b) $\theta = 87°$; and (c) $\theta = 135°$.

3.2. Predictions based on dimensional analysis

The parameters influencing the fundamental resonance frequency are the geometric and flow parameters, L, S, p_0, and ρ_0. The following two dimensionless groups Π_1 and Π_2 can be formed from these parameters:

$$\Pi_1 = \frac{P_0}{\rho_0 f^2 L^2}, \quad \Pi_2 = \frac{P_0}{\rho_0 f^2 S^2} \tag{2}$$

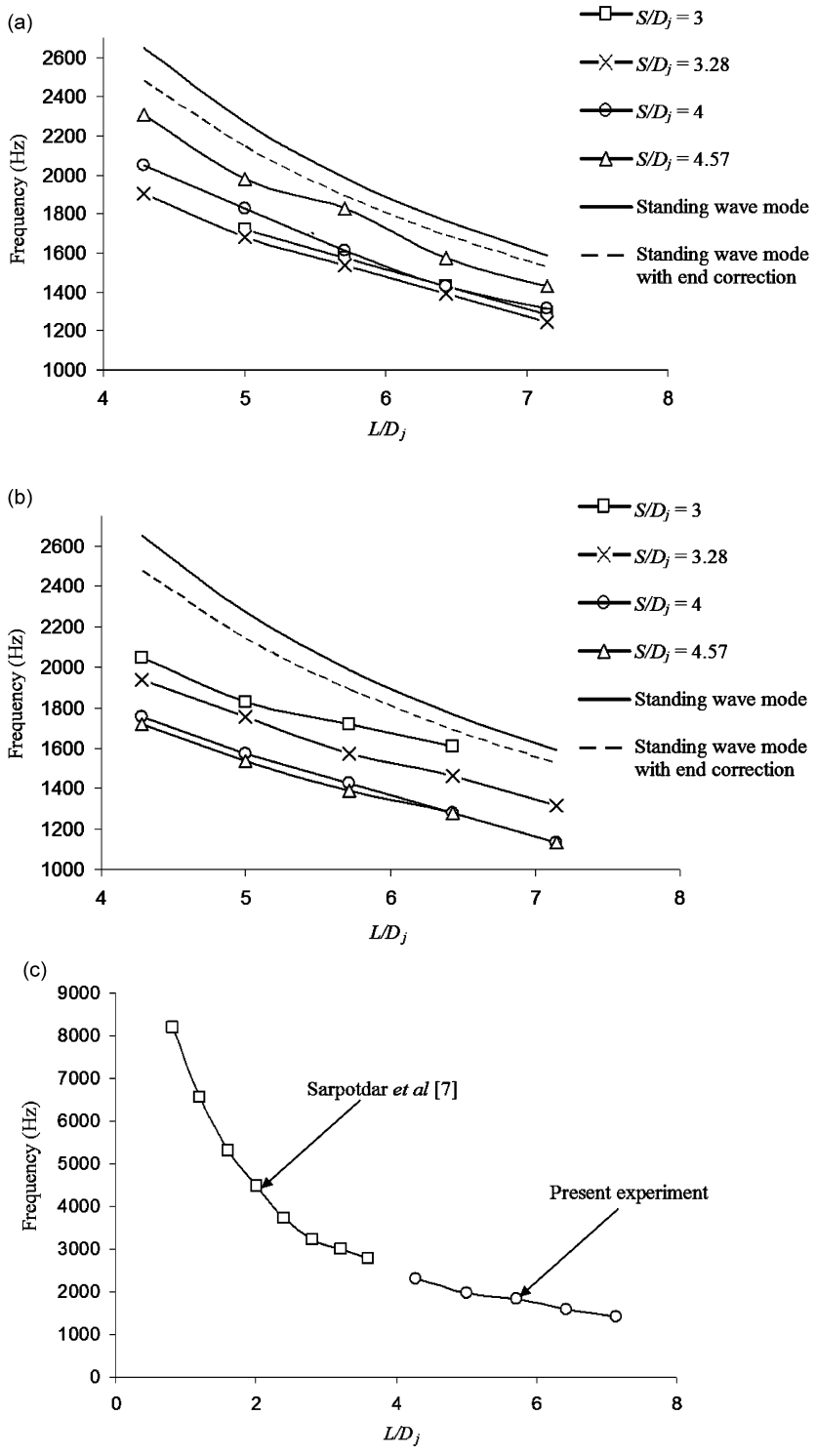

Fig. 6. Variation of fundamental frequency with cavity length: (a) $R = 4.92$, (b) $R = 5.91$, and (c) comparison of frequencies at $S/D_j = 4.57$, $R = 4.92$ with Sarpotdar et al. [7] at $S/D_j = 1.5$, $R = 4.29$.

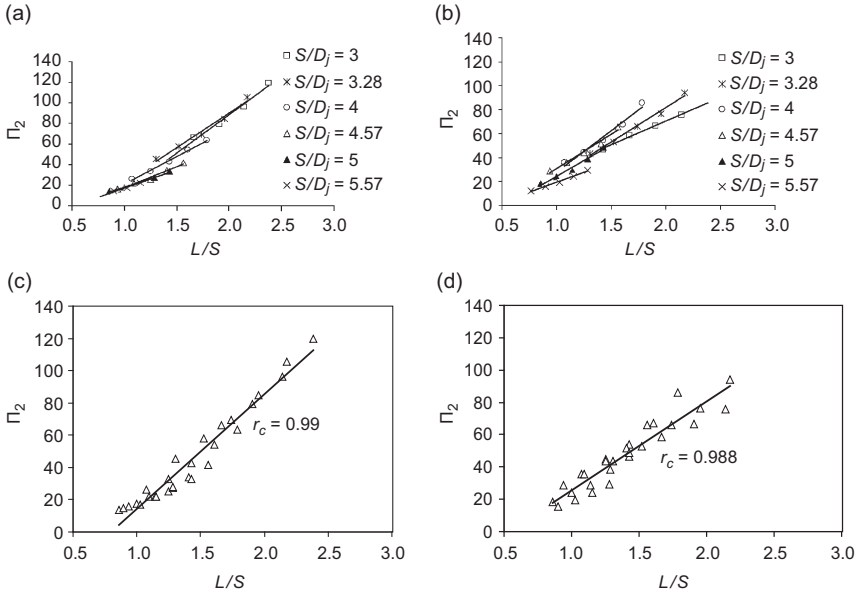

Fig. 7. Variation of dimensionless number Π_2 with L/S for various stand-off distances (a, c) $R = 4.92$ and (b, d) $R = 5.91$.

The dimensionless numbers Π_1 and Π_2 when plotted against the non-dimensional parameters such as L/S, L/D_j, S/D_j and R, could provide clues for the combination of parameters controlling the frequency. The value of Π_2 was found to monotonically increase with L/S, while no specific dependence could be obtained for the variation of Π_1 with L/S, L/D_j, S/D_j or R. The linear correlation for Π_2 is shown in Fig. 7 for R values of 4.92 and 5.91. A linear fit gave a correlation factor r_c greater than 0.97, strongly suggesting the linear dependence of Π_2 with L/S. However, it may be noted that in very small length cavities, errors would be large because the end-effects become significant.

The parameter Π_2 could be written in terms of the stagnation sound speed as $C_0^2/\gamma f^2 S^2$, and the linear variation with L/S (Fig. 7) suggests that

$$\frac{C_0^2}{\gamma f^2 S^2} = a_1(L/S) + a_2 \tag{3}$$

where a_1 and a_2 are obtained from the experimental data of Fig. 7(c,d). Simplifying Eq. (3), we obtain the frequency to be of the form

$$f = \frac{C}{\sqrt{\gamma S(a_1 L + a_2 S)}} \tag{4}$$

The above expression is similar to the frequency of a classical Helmholtz resonator

$$f = \frac{C}{2\pi}\sqrt{\frac{A_{\text{neck}}}{V L_{\text{neck}}}} = \frac{C}{2\pi}\sqrt{\frac{1}{(V/A_{\text{neck}})L_{\text{neck}}}} \tag{5}$$

In Eq. (4), the stand-off distance S is analogous to L_{neck} and the distance parameter $(a_1 L + a_2 S)$ is analogous to V/A_{neck}. The parametric study suggests that the whistle operates in a mode similar to a Helmholtz resonator with probably the barrel-shock oscillations driving the resonance. A schematic of the mechanism is depicted in Fig. 8.

While a Helmholtz resonator has one oscillating fluid column, the present problem involves two oscillating fluid columns. One corresponds to the shock cell and the other, the fluid in the cavity. These two oscillating columns can in turn be characterized by their respective Helmholtz numbers. In our study, the two non-dimensional parameters Π_1 and Π_2 are slightly modified forms of the corresponding Helmholtz numbers for

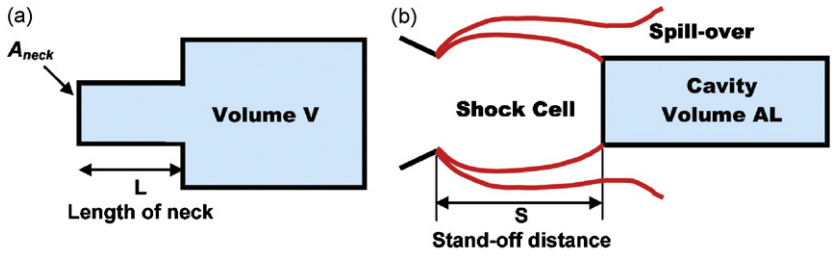

$$f = \frac{C}{2\pi}\sqrt{\frac{A_{neck}}{VL}} \qquad f = \frac{C}{2\pi}\sqrt{\frac{A_{neck}}{A_{neck}LS}}$$

$$f = \frac{C}{\sqrt{\gamma\, S(a_1 L + a_2 S)}}$$

Fig. 8. Analogy between classical Helmholtz resonator and Hartmann whistle. (a) Classical Helmholtz resonator and (b) interaction of jet with cavity.

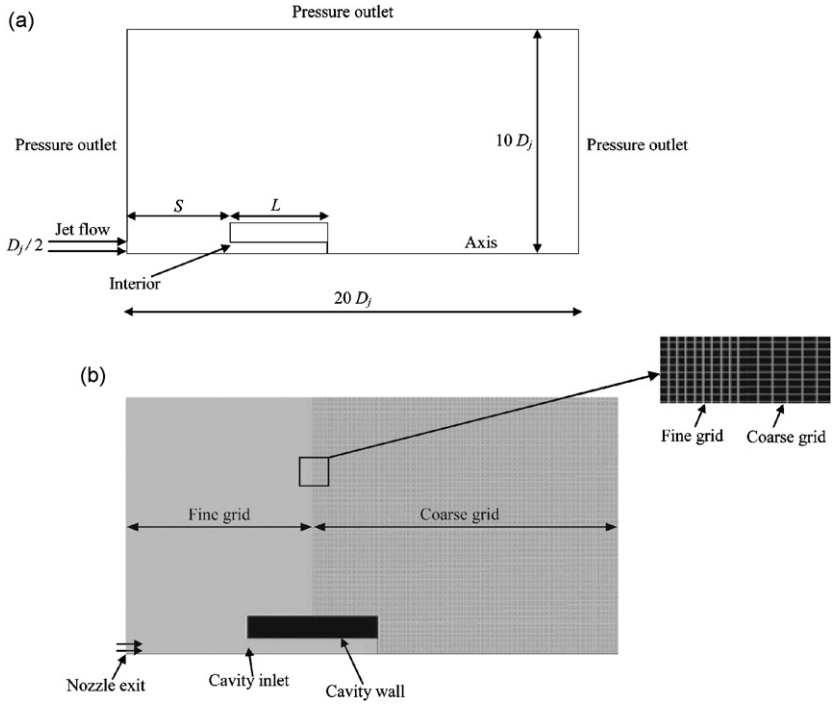

Fig. 9. (a) Computational domain and boundary conditions and (b) computational grid.

the two oscillating columns. Numerical simulations were carried out to determine the flow structure accompanying the oscillations. The results of the simulation are given in the next section.

3.3. Numerical simulation of jet flow interaction with cavity

The boundary conditions for the jet flow simulation are shown in Fig. 9(a). The nozzle dimensions are very small and it is difficult to measure the actual velocity profiles at the jet inlet. Considering the convergent portions in the settling chamber and nozzle preceding the throat, a choked uniform flow condition is

prescribed at the exit of the nozzle. It must be noted that the nozzle is operated in the underexpanded mode. The nozzle exit pressure is calculated based on isentropic relations.

Grids with number of cells varying from approximately 250 000–400 000 were generated using the GAMBIT software for different stand-off distances. The computational grid with varying mesh size is shown in Fig. 9(b). Fine grids were used where shock cells exist. The boundary layer near the cavity wall is resolved by restricting the maximum wall y^+ value within about 100.

A transient axisymmetric simulation was carried out using FLUENT 6.2 with an implicit segregated solver. The Spalart–Allmaras turbulence model with the standard values of model constants ($C_{b1} = 0.1355$; $C_{b2} = 0.622$; $C_{v1} = 7.1$; $C_{w2} = 0.3$; $C_{w3} = 2$, $\sigma_{\tilde{v}} = \frac{2}{3}$) was used for modeling turbulence. The Spalart–Allmaras turbulence model [18] is a relatively simple one-equation model which has been shown to give good results for wall-bounded flows and boundary layers subjected to adverse pressure gradients.

A grid sensitivity study was carried out by varying the number of cells as: 197 522, 290 909 and 396 728. This study revealed that the current results obtained with 249 874 cells for small $S/D_j = 2.86$ and 396 728 cells for large $S/D_j = 4.57$ are almost invariant to further grid refinement. The variation of static pressure with position along the axis for various grids is shown in Fig. 10. During computations, initially, the mass flow rate into the cavity was observed to undergo rapid oscillations. After this initial transient period, the flow structure in the vicinity of the cavity is examined for the presence or absence of regurgitance. These studies reveal that jet regurgitance is predominant in cases where stand-off distance is small and weaker for large stand-off distances.

Results are presented for two cases corresponding to small and large stand-off distances. Fig. 11 shows the flow structure for $L/D_j = 4.28$, $S/D_j = 4.57$, $R = 5.91$. For this case with large stand-off distance, steady-state velocity vectors illustrate that most of the jet flow gets diverted around the cavity, by the prevailing shock-structure. In this case, the resonance is a result of fluid column oscillations in the shock-cell and cavity regions and not due to flow regurgitance. Recirculation zones are visible at the mouth of the cavity which also play an important role in diverting the flow. The Mach contours shown in Fig. 11(b) indicate regions of flow deceleration and re-acceleration. In particular, the expansion fans of the underexpanded jet flow followed by the coalescence of compression waves into a Mach disk (A in Fig. 11(b)), are clearly depicted in the figure. Following the Mach disk, the flow re-accelerates (B) and is diverted away by a conical oblique shock (C) located at the mouth of the cavity. Flow re-circulation zones (D) are observed at the mouth of the cavity.

Fig. 12(a)–(e) shows the flow structure for $L/D_j = 4.28$, $S/D_j = 2.86$, $R = 4.92$, at various time instances. These figures depict one full cycle of regurgitant oscillations. The in-flow into the cavity just begins at the instance ($t = 0.1$ ms) shown in Fig. 12(a), and it grows in strength as shown for $t = 0.2$ ms in Fig. 12(b). The beginning of out-flow from the cavity is seen for $t = 0.3$ ms, and it grows in strength by $t = 0.4$ ms as shown in Fig. 12(c) and (d), respectively. The flow structure returns to the original state at $t = 0.5$ ms as shown in Fig. 12(e). The figures also include Mach number contours alongside for each time instance. As seen from the Mach number contours, the maximum Mach number for forward or return flow is about 0.6. This illustrates that at smaller stand-off distances, regurgitance plays an active role in the resonant oscillations. The

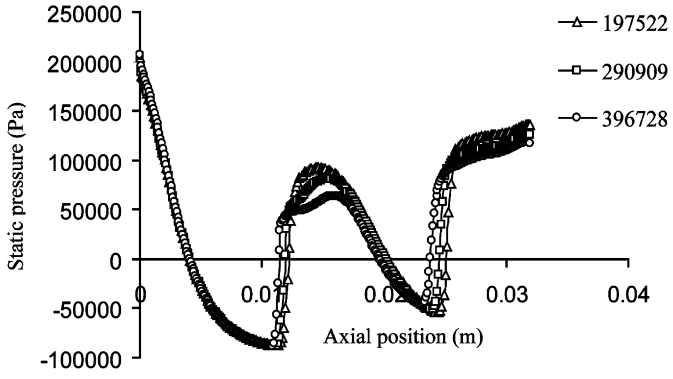

Fig. 10. Axial variation of static pressure for various grids representing grid sensitivity.

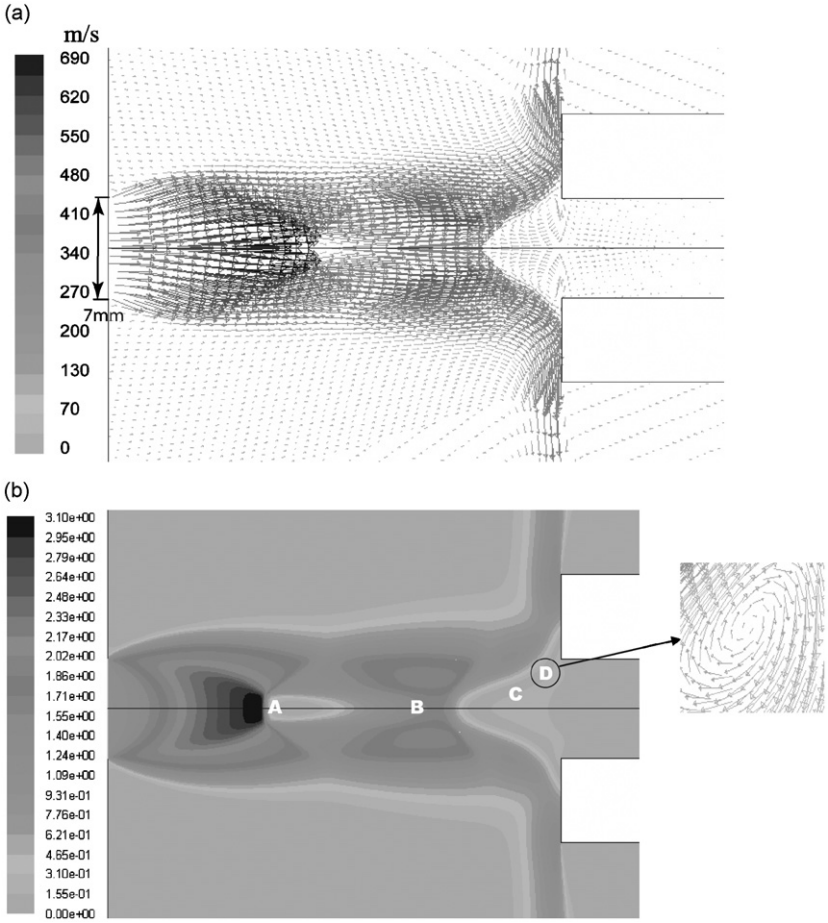

Fig. 11. Steady-state predictions for $L/D_j = 4.28$, $S/D_j = 4.57$, $R = 5.91$: (a) velocity vectors and (b) Mach number contours.

fundamental frequency predicted by the simulation is compared with corresponding experimental value for two cases, as shown in Table 1. In this table, the stand-off distance for case 1 is smaller than that of case 2, and hence strong regurgitance is seen for case 1 only (Fig. 12). The agreement of fundamental frequencies for both the strong and weak regurgitating cases is seen to be good.

4. Directivity and power studies

Fig. 13 shows the directivity of the acoustic intensity as measured in the various experiments. The whistle was found to be highly directive in the downstream direction. The intensity was higher for smaller cavity lengths with the other parameters remaining constant and this is brought out in Fig. 13(a). Smaller stand-off distances led to larger intensities as observed from Fig. 13(b). Brocher et al. [2] had also obtained maximum amplitude of oscillations for supersonic jet flow for $S/D_j \approx 2$. The acoustic intensity was observed to be higher with increasing R (Fig. 13(c)). The figure also compares the directivities of whistle and free jet for different values of R. It is observed that the whistle intensities are much higher than those of free jets. However, the common feature between the two is their downstream directivity. The free jet directivity is maximum around 30° while that of the whistle is around $35–45^\circ$ due to the flow diversion induced by the cavity. This reiterates the fact that the Hartmann whistle is an efficient acoustic generator.

Tonal sound pressure level plots are shown in Fig. 14. Odd harmonics (f, $3f$) are seen to be more directive in the downstream side while the even harmonics ($2f$, $4f$) are directive in the upstream direction. Higher

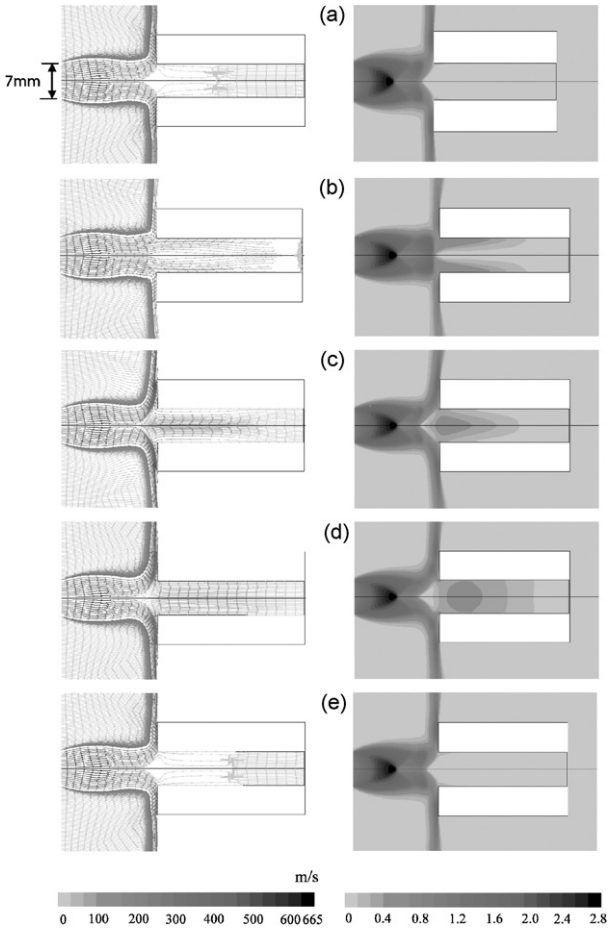

Fig. 12. Transient velocity vectors and Mach number contours within a cycle for $L/D_j = 4.28$, $S/D_j = 2.86$, $R = 4.92$: (a) 0.1 ms; (b) 0.2 ms; (c) 0.3 ms; (d) 0.4 ms; and (e) 0.5 ms.

Table 1
Comparison of fundamental frequency obtained from experiment and simulation.

Sl. no.	Parameters	Frequency in experiments (Hz)	Frequency in computations (Hz)	Percentage deviation
1.	$R = 4.92$ $S/D_j = 2.86$ $L/D_j = 4.28$	1978	2100	6.17
2.	$R = 5.91$ $S/D_j = 4.57$ $L/D_j = 4.28$	1721	1660	3.54

harmonics such as $5f$, $6f$, $7f$, and $8f$ also gave the same trends and these observations suggest that directivity downstream may be generalized as taking place for odd harmonics. Raman and Rice [19] have shown that for rectangular jets, depending upon the instability mode being symmetric or antisymmetric, directivities of the fundamental component and harmonics can be different. In the present experiments, the shock cells in the underexpanded jet flow and the regurgitant flow/cavity column oscillations could behave as coupled acoustic sources. Depending upon the type of coupling, the directivities of various harmonics could be different.

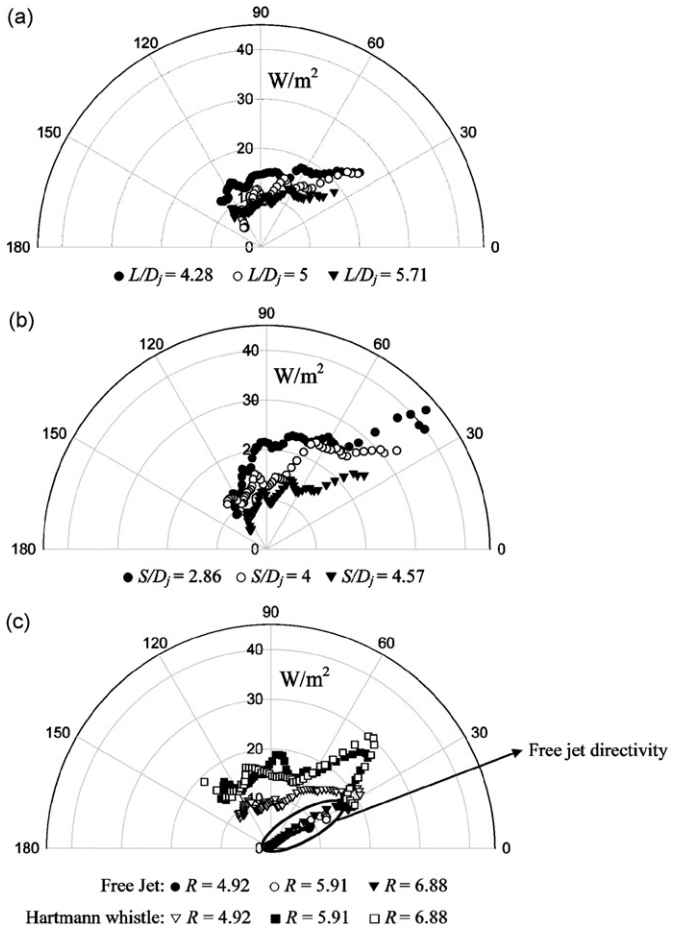

Fig. 13. Directivities of acoustic intensity: (a) variation with L/D_j for $S/D_j = 4.57$ and $R = 4.92$; (b) variation with S/D_j, for $L/D_j = 5$ and $R = 4.92$; and (c) comparison of intensity directivity of Hartmann whistle at $S/D_j = 4.57$ and $L/D_j = 5$ with free jet at different R.

Fig. 15(a) shows the variation of slice power directivity and this is also seen to be higher for small cavity lengths. Fig. 15(b) shows the variation of power for different values of R. The slice power directivity increases with R. The dimensional analysis mentioned earlier also yielded a dimensionless group involving the acoustic power, as follows:

$$\Pi_3 = \frac{P}{D_j^3 f p_0} \tag{6}$$

This dimensionless number is plotted against the stand-off distance and cavity length in Fig. 16. Smaller values of stand-off distances and larger cavity lengths enhance acoustic power.

Fig. 17 shows the variation of acoustic efficiency with the dimensionless cavity length and stand-off distance, at a fixed pressure ratio of $R = 4.92$. For the sake of comparison, the acoustic efficiency of free jet at the same pressure ratio is also determined and is observed to be only 0.16%. It is evident that the acoustic efficiency of the whistle is typically an order of magnitude higher at all cavity lengths and stand-off distances. This corroborates the fact that the cavity indeed serves as a strong acoustic intensifier. At smaller stand-off distances, the acoustic efficiency is higher. As S/D_j increases the number of shock cells also increases and the jet spreads more, before reaching the cavity. These factors lead to more diversion of flow sideways. This in conjunction with a smaller cavity volume (smaller L/D_j) leads to a smaller fraction of flow participating in the cavity fluid oscillations. In turn, the acoustic power drops at combinations of large S/D_j with small L/D_j.

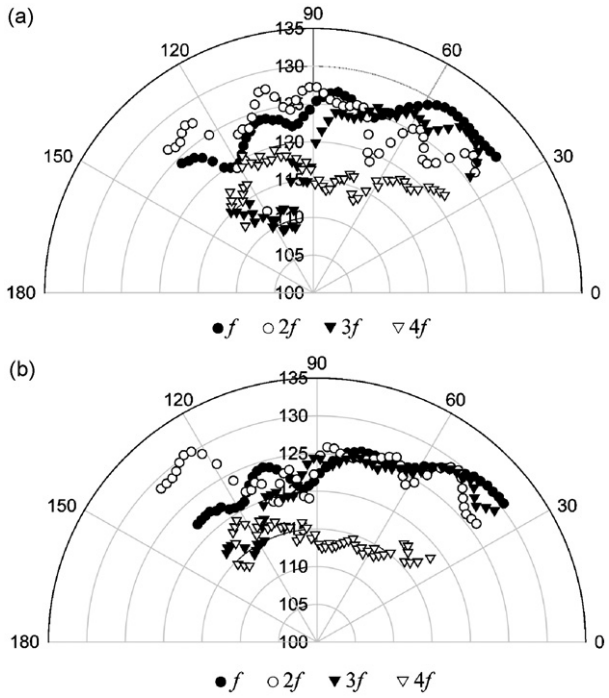

Fig. 14. Variation of tonal SPL in dB at $L/D_j = 4.28$ and $R = 4.92$ for: (a) $S/D_j = 2.86$, and (b) $S/D_j = 3.28$.

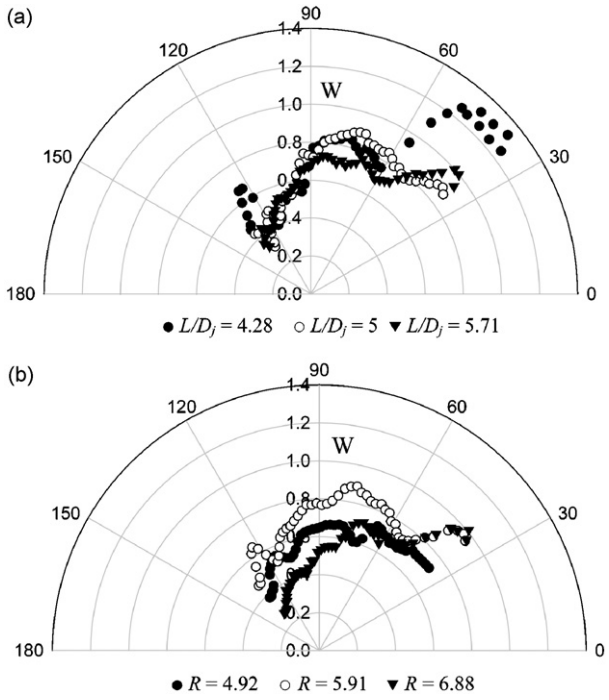

Fig. 15. Acoustic slice power directivity: (a) variation with L/D_j for $R = 4.92$ and $S/D_j = 3.28$; and (b) variation with R for $S/D_j = 4.57$ and $L/D_j = 4.28$.

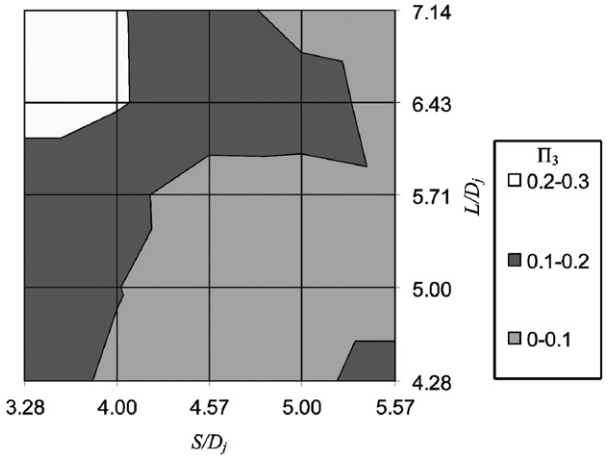

Fig. 16. Variation of non-dimensional acoustic power Π_3 with cavity length and stand-off distance.

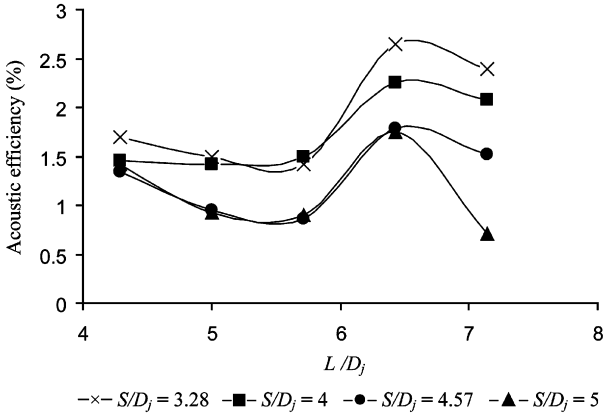

Fig. 17. Variation of acoustic efficiency with cavity length.

For any stand-off distance, the acoustic efficiency exhibits a decreasing and increasing trend with respect to cavity length. This may be attributed to the complex interactions between the two oscillating columns of the shock-cell and the cavity fluid. For very small cavity lengths, the volumetric capacitance is low leading to low efficiencies. On the other hand, for very long cavities, damping effects will become too high resulting in low acoustic efficiency. For some intermediate length, the acoustic efficiency is expected to be maximum. In the range of parameters studied, it is seen that maximum acoustic efficiency is attained at L/D_j of around 6.5.

5. Conclusions

A detailed characterization of the interaction of the jet flow with the cylindrical cavity in a Hartmann whistle is carried out. Experiments are done for values of pressure ratio of the jet between 4.92 and 6.88 with variations in the stand-off distance and cavity length. The spectra, sound pressure level, and directivity are determined, correlated with theory, and supplemented by numerical computations.

Distinct spectra corresponding to the standing wave modes of the cavity modulated by the stand-off distance are shown to be excited over the entire range of pressure ratios of the experiments. The fundamental frequency is much lower than the jet screech frequencies and the frequencies determined using the quarter wavelength theory. A theoretical model based on dimensional analysis shows that the fundamental frequency for the whistle can be calculated using the Helmholtz resonator analogy with the stagnation sound velocity,

stand-off distance, and the length of the cavity as parameters. The frequency predicted with this model is in excellent agreement with the experimental findings.

Numerical computations reveal that cavity stand-off distance is a crucial parameter that determines the existence of jet regurgitant mode. This mode is significant at smaller stand-off distances. Directivity of the acoustic radiation from the whistle is in the downstream direction at an angle between 35° and 45° measured from the downstream axis. As compared to a free jet, which has a directivity at 30°, the directivity at higher angles for the whistle is seen to arise from the flow diversion at the cavity mouth. Directivities of tonal sound pressure levels reveal that odd harmonics are directive in the downstream direction compared to even harmonics which are directive in the upstream direction.

In general, smaller stand-off distances, larger cavity lengths and higher pressure ratios result in larger acoustic intensities. The acoustic efficiency of the whistle is higher by about one order of magnitude as compared to that of a free jet. Maximum acoustic efficiencies are obtained for cavity length to jet diameter ratios of around 6.5 for all stand-off distances.

References

[1] V. Sarohia, H.L. Back, Experimental investigation of flow and heating in a resonance tube, *Journal of Fluid Mechanics* 94 (4) (1979) 649–672.
[2] E. Brocher, C. Maresca, M.H. Bournay, Fluid dynamics of the resonance tube, *Journal of Fluid Mechanics* 43 (2) (1970) 369–384.
[3] J. Iwamoto, Experimental study of flow oscillation in a rectangular jet driven tube, *Journal of Fluids Engineering—Transactions of the American Society of Mechanical Engineers* 112 (1) (1990) 23–27.
[4] G.B. Sobeiraj, A.P. Szumowsky, Experimental investigations of an underexpanded jet from a convergent nozzle impinging on a cavity, *Journal of Sound and Vibration* 149 (3) (1991) 375–396.
[5] J. Kastner, M. Samimy, Development and characterization of Hartmann tube fluidic actuators for high-speed control, *American Institute of Aeronautics and Astronautics Journal* 40 (10) (2002) 1926–1934.
[6] G. Raman, E. Envia, T.J. Bencic, Jet cavity interaction tones, *American Institute of Aeronautics and Astronautics Journal* 40 (8) (2002) 1503–1511.
[7] S. Sarpotdar, G. Raman, A.B. Cain, Powered resonance tubes: resonance characteristics and actuation signal directivity, *Experiments in Fluids* 39 (6) (2005) 1084–1095.
[8] G. Raman, S. Khanafseh, A.B. Cain, E. Kerschen, Development of high bandwidth powered resonance tube actuators with feedback control, *Journal of Sound and Vibration* 269 (3–5) (2004) 1031–1062.
[9] J.W. Gregory, J.P. Sullivan, Characterization of Hartmann tube flow with porous pressure-ensitive paint, *33rd AIAA Fluid Dynamics Conference and Exhibit*, June 23–26, 2003, Orlando, FL, 2003, AIAA-2003-3713.
[10] E. Brun, R.M.G. Boucher, Research on the acoustic air-jet generator: a new development, *Journal of the Acoustical Society of America* 29 (5) (1957) 573–583.
[11] S. Murugappan, E. Gutmark, Parametric study of the Hartmann–Sprenger tube, *Experiments in Fluids* 38 (6) (2005) 813–823.
[12] A. Hamed, K. Das, D. Basu, Characterization of powered resonance tube for high frequency excitation, *Proceedings of FEDSM'03 4TH ASME–JSME Joint Fluids Engineering Conference Honolulu*, July 6–11, 2003, Hawaii, USA, 2003, FEDSM 2003-45472.
[13] A. Hamed, K. Das, D. Basu, Numerical simulation and parametric study of Hartmann Sprenger tube based powered device, *American Institute of Aeronautics and Astronautics*, AIAA-2003-0550.
[14] K.S. Chang, K.H. Kim, J. Iwamoto, A study on the Hartmann Sprenger tube flow driven by a sonic jet, *International Journal of Turbo and Jet Engines* 13 (1996) 173–182.
[15] J.M. Seiner, *Advances in high speed jet aeroacoustics*, AIAA-84-2275.
[16] G. Raman, Cessation of screech in underexpanded jets, *Journal of Fluid Mechanics* 336 (1997) 69–90.
[17] J. Hartmann, B. Trolle, A new acoustic generator. The air-jet generator, *Journal of Scientific Instruments* 4 (4) (1927) 101–111.
[18] P. Spalart, S. Allmaras, A one-equation turbulence model for aerodynamic flows, *American Institute of Aeronautics and Astronautics*, Technical Report AIAA-92-0439.
[19] G. Raman, E.J. Rice, Instability modes excited by natural screech tones in a supersonic rectangular jet, *Physics of Fluids* 6 (12) (1994) 3999–4008.